

FAB: An FPGA-based Accelerator for Bootstrappable Fully Homomorphic Encryption

Rashmi Agrawal¹ Leo de Castro² Guowei Yang¹ Chiraag Juvekar³ Rabia Yazicigil¹
Anantha Chandrakasan² Vinod Vaikuntanathan² Ajay Joshi¹

¹Boston University, Boston MA, USA; ²MIT, Cambridge, MA, USA; ³Analog Devices, Boston, MA USA
{rashmi23, guoweiy, rty, joshi}@bu.edu, {ldec, anantha, vinodv}@mit.edu, chiraag.juvekar@analog.com

ABSTRACT

Fully Homomorphic Encryption (FHE) offers protection to private data on third-party cloud servers by allowing computations on the data in encrypted form. However, to support general-purpose encrypted computations, all existing FHE schemes require an expensive operation known as “bootstrapping”. Unfortunately, the computation cost and the memory bandwidth required for bootstrapping add significant overhead to FHE-based computations, limiting the practical use of FHE.

In this work, we propose FAB, an FPGA-based accelerator for bootstrappable FHE. Prior FPGA-based FHE accelerators have proposed hardware acceleration of basic FHE primitives for impractical parameter sets without support for bootstrapping. FAB, for the first time ever, accelerates bootstrapping (along with basic FHE primitives) on an FPGA for a secure and practical parameter set. Prior hardware implementations of FHE that included bootstrapping are heavily memory bound, leading to large execution times and wasted compute resources. The key contribution of our work is to architect a balanced FAB design, which is not memory bound. To this end, we leverage recent algorithms for bootstrapping while being cognizant of the compute and memory constraints of our FPGA. To architect a balanced FAB design, we use a minimal number of functional units for computing, operate at a low frequency, leverage high data rates to and from main memory, utilize the limited on-chip memory effectively, and perform operation scheduling carefully.

We evaluate FAB using a single Xilinx Alveo U280 FPGA and by scaling it to a multi-FPGA system consisting of eight such FPGAs. For bootstrapping a fully-packed ciphertext, while operating at 300 MHz, FAB outperforms existing state-of-the-art CPU and GPU implementations by $213\times$ and $1.5\times$ respectively. Our target FHE application is training a logistic regression model over encrypted data. For logistic regression model training scaled to 8 FPGAs on the cloud, FAB outperforms a CPU and GPU by $456\times$ and $6.5\times$, and provides competitive performance when compared to the state-of-the-art ASIC design at a fraction of the cost.

1. INTRODUCTION

The last decade has seen rapid growth in machine learning (ML) with exciting ML-based applications in a variety of fields. Given the sheer amount of data that is used by these applications, ML accelerators on the cloud [46, 32] offer a way to accelerate the performance of each phase (data storage, training, and inference) in ML. However, these cloud-

based accelerators also introduce privacy concerns by providing unrestricted access to the data to third-party cloud servers.

Fully homomorphic encryption (FHE) [40, 19] is currently regarded as the “gold standard” to preserve the privacy of data while enabling machine learning training/inference in an untrusted cloud environment. FHE enables computing on data *while it is encrypted*, allowing the cloud to operate on the data without having access to the data itself. Despite this incredible achievement of theoretical cryptography, the large compute and memory requirements of FHE remain a serious barrier to its widespread adoption. For example, to train a logistic regression (LR) model for 30 iterations using plaintext data (11,982 samples with 196 features), it takes ~ 1.05 sec on a CPU. The same LR model training on encrypted data takes ~ 124 mins on the same CPU [26], a slowdown of about $7086\times$. At the same time, the size of encrypted data (198 MB) used in this training is $152\times$ larger than the size of the plaintext data (1.3 MB).

To address the compute and memory requirements of FHE, several optimizations and acceleration efforts are in progress. For FHE-based computing on CPUs, SEAL [42], PALISADE [43], HELib [29, 23], NFFLib [1], Lattigo [36], and HEAAN [33] software libraries accelerate one or more FHE schemes. Unfortunately, CPUs do not have the capability to adequately exploit the inherent parallelism available in FHE. GPU-based FHE accelerators [14, 2, 31] have recently had more success. These GPU-based implementations exploit the inherent parallelism in FHE, but the GPUs have massive floating-point units that are completely underutilized as FHE-based workloads consist almost entirely of integer-only operations. Moreover, neither CPU nor GPU can provide adequate main memory bandwidth to handle the data-intensive nature of the FHE-based workloads.

Consequently, Samardzic et al. [41] and Kim et al. [35] proposed custom FHE accelerators called F1 and BTS, respectively. Both accelerators are highly resource-intensive, requiring a massive number (8192-18432) of processing elements and large on-chip memory (64-512 MB) to accelerate FHE workloads. Despite these resources, neither F1 nor BTS is able to store the entire working set of FHE-based workloads. Effectively, these proposals are still bottlenecked by main memory bandwidth. Since main memory cannot keep up with the custom ASIC implementations of F1 and BTS, this leads to the compute portions of these accelerators sitting idle. A more in-depth discussion of these related works is in Section 6. At a high-level, neither of these ASIC proposals overcome the fundamental barrier of mem-

ory bandwidth, which limits their performance.

In this work, we propose FAB, an FPGA-based accelerator for bootstrappable FHE that supports the Cheon-Kim-Kim-Song (CKKS) [12] FHE scheme. FAB makes use of state-of-the-art analysis of the bootstrapping algorithm [15] to co-design the FHE operations and select parameters that are optimized for the hardware constraints. This allows FAB to support practical FHE parameter sets (i.e. parameters large enough to support bootstrapping) *without* being bottlenecked by the main-memory bandwidth. This does not come at the cost of compute efficiency. We evaluate FAB on a target application of training a logistic regression model over encrypted data. Our benchmarks demonstrate that FAB outperforms all prior works ($6.5\times$ to $456\times$) and is competitive with the state-of-the-art ASIC proposal. More details on our evaluation are in Section 5.

We architect FAB for the Xilinx Alveo U280 FPGA accelerator card containing High Bandwidth Memory 2 (HBM2). FAB is highly resource efficient, implementing only 256 functional units, where each functional unit supports various modular arithmetic operations. FAB exploits maximal pipelining and parallelism by utilizing these functional units as per the computational demands of the FHE operations. FAB also makes efficient use of the limited 43 MB on-chip memory and a 2 MB register file to manage the >100 MB working dataset at any given point of time. Moreover, FAB leverages a smart operation scheduling to enable higher data reuse and prefetching of the required datasets from main memory without stalling the functional units. In addition, this smart scheduling evenly distributes the accesses to main memory so as to efficiently utilize the limited main memory bandwidth through a homogeneous memory traffic. A detailed description of the microarchitecture of FAB is given in Section 4.

The performance of FAB suggests that FPGA is a “sweet-spot” for FHE acceleration. FAB significantly outperforms both CPU and GPU implementations of FHE. In contrast to ASICs, FAB only uses standard, commercially available hardware that is highly accessible to the general public (e.g. via the AWS F1 cloud). By enabling near-ASIC levels of performance with the same availability as a high-end GPU, FAB demonstrates that FPGAs are the most viable option for near-term hardware acceleration of FHE. Furthermore, FAB effectively raises the bar for the performance of future ASIC proposals since the advantage of the current state-of-the-art ASIC proposal over FAB is not worth the millions of dollars of investment required to fabricate a custom hardware chip.

In summary, we make the following contributions:

- We propose FAB, a novel accelerator that supports all homomorphic operations, including fully-packed bootstrapping, in the CKKS FHE scheme for practical FHE parameters. This accelerator outperforms all prior works and is competitive with the latest ASIC proposals for our target application: secure training of logistic regression models.
- FAB tackles the memory-bounded nature of bootstrappable FHE through smart operation scheduling and on-chip memory management techniques, in turn maximizing the overall FHE-based computing throughput.
- Last but not least, FAB uses only currently-existing hard-

Table 1: CKKS FHE Parameters and their description.

Parameter	Description
N	Number of coefficients in the ciphertext polynomial.
n	Number of plaintext elements in a ciphertext ($n \leq N/2$ is required).
Q	Full modulus of a ciphertext coefficient.
q	Prime modulus and a limb of Q .
L	Maximum number of limbs in a ciphertext.
ℓ	Current number of limbs in a ciphertext.
dnum	Number of digits in the switching key.
α	$\lceil (L + 1)/\text{dnum} \rceil$. Number of limbs that comprise a single digit in the key-switching decomposition. This value is fixed throughout the computation.
P	Product of the extension limbs added for the raised modulus. There are $\alpha + 1$ extension limbs.
fftIter	Multiplicative depth of a linear transform in bootstrapping.

ware (FPGAs), and *does not require any custom hardware*. This makes FAB immediately accessible to the general public as all of the resources required to support FAB exist in public commercial cloud environments (e.g. AWS F1 instances). In short, FAB offers performance that is competitive with ASIC with the accessibility of a pure CPU/GPU implementation, and demonstrates FPGAs to be a sweet-spot for bootstrappable FHE.

2. BACKGROUND

In this section, we briefly review the CKKS [12] homomorphic encryption scheme and the relevant parameters for FAB. A summary of these parameters is given in Table 1.

2.1 The CKKS FHE Scheme

The CKKS [12] scheme supports operations over vectors of complex numbers. A plaintext in the CKKS scheme is an element of \mathbb{C}^n , where \mathbb{C} is the field of complex numbers. The plaintext operations are component-wise addition and component-wise multiplication of elements of \mathbb{C}^n . In addition to the plaintext size n , CKKS is parameterized by a ciphertext coefficient modulus $Q \in \mathbb{Z}$ (where \mathbb{Z} is the ring of integers) and a ciphertext polynomial modulus $x^N + 1$, where N is chosen to be a power of 2. CKKS ciphertexts are elements of \mathcal{R}_Q^2 , where $\mathcal{R}_Q := \mathbb{Z}_Q[x]/(x^N + 1)$. We denote the encryption of a vector $\mathbf{m} \in \mathbb{C}^n$ by $\llbracket \mathbf{m} \rrbracket = (\mathbf{a}_m, \mathbf{b}_m)$ where \mathbf{a}_m and \mathbf{b}_m are the two elements of \mathcal{R}_Q that comprise the ciphertext.

CKKS supports the following operations over encrypted vectors. All arithmetic operations between two plaintext vectors are *component-wise*.

- $\text{Add}(\llbracket \mathbf{m}_1 \rrbracket, \llbracket \mathbf{m}_2 \rrbracket) \rightarrow \llbracket \mathbf{m}_1 + \mathbf{m}_2 \rrbracket$, where the addition is component-wise over \mathbb{C} .

- $\text{Mult}([\mathbf{m}_1], [\mathbf{m}_2]) \rightarrow [\mathbf{m}_1 \odot \mathbf{m}_2]$, where \odot represents the component-wise product of two vectors.
- $\text{Rotate}([\mathbf{m}], k) \rightarrow [\phi_k(\mathbf{m})]$, where ϕ_k is the function that rotates a vector by k entries. As an example, when $k = 1$, the rotation $\phi_1(\mathbf{x})$ is defined as follows:

$$\begin{aligned} \mathbf{x} &= (x_0 \ x_1 \ \dots \ x_{n-2} \ x_{n-1}) \\ \phi_1(\mathbf{x}) &= (x_{n-1} \ x_0 \ \dots \ x_{n-3} \ x_{n-2}) \end{aligned}$$

- $\text{Conjugate}([\mathbf{m}]) \rightarrow [\overline{\mathbf{m}}]$ where $\overline{}$ represents the complex conjugate operation.

2.1.1 Homomorphic Levels & RNS Representation

To efficiently operate over elements of \mathcal{R}_Q , we represent Q as a product of primes q_1, \dots, q_ℓ where each q_i is roughly the size of a machine word. This follows the standard residue number system (RNS) representation of ciphertext moduli [24, 11]. We call each q_i a *limb* of the modulus Q , and we say a modulus $Q := \prod_{i=1}^{\ell} q_i$ has $\ell - 1$ levels. We call the set $\mathcal{B} := \{q_1, \dots, q_\ell\}$ an *RNS basis*. Each multiplication operation reduces the size of the modulus by one limb. A modulus with ℓ levels can support a circuit of multiplicative depth ℓ before bootstrapping is required. Addition, rotation, and conjugation operations do not change the number of levels in a modulus.

This representation allows us to operate over values in \mathbb{Z}_Q without any native support for multi-precision arithmetic. Instead, we can represent $x \in \mathbb{Z}_Q$ as a length- ℓ vector of scalars $[x]_{\mathcal{B}} = (x_1, x_2, \dots, x_\ell)$, where $x_i \equiv x \pmod{q_i}$. We refer to each x_i as a *limb* of x . To add two values $x, y \in \mathbb{Z}_Q$, we have $x_i + y_i \equiv x + y \pmod{q_i}$. Similarly, we have $x_i \cdot y_i \equiv x \cdot y \pmod{q_i}$. This allows us to compute addition and multiplication over \mathbb{Z}_Q while only operating over standard machine words.

We briefly define the equation for RNS recombination. We refer the reader to [24, 11] for more details. This equation takes in an RNS representation of a value $x \in \mathbb{Z}_Q$ as a length- ℓ vector of scalars $[x]_{\mathcal{B}} = (x_1, x_2, \dots, x_\ell)$, where $x_i \equiv x \pmod{q_i}$. It outputs $x \pmod{p}$, where p is a new modulus in an extended RNS basis.

$$[x]_p = \sum_{i=1}^{\ell} [x_i \cdot \tilde{Q}_i]_{q_i} \cdot Q_i^* \pmod{p} \quad (1)$$

where $Q_i^* = Q/q_i$ and $\tilde{Q}_i = (Q_i^*)^{-1} \pmod{q_i}$

In memory, ciphertext data can be viewed as an $\ell \times n$ matrix, where each row is a limb and each column corresponds to a single coefficient modulo Q . Arranging this matrix in "row-major order" where there is locality for elements in the same row is called *limb-wise* access, since it enables efficient data within a single limb. By contrast, arranging this matrix in "column-major order" where there is locality for elements in the same column is known as *slot-wise* access, since it is best for accessing the same slot of data across all of the ciphertext limbs.

2.1.2 Number Theoretic Transform

To efficiently multiply elements of \mathcal{R}_Q , we make use of the number theoretic transform (NTT), which is the analog

of the Fast Fourier Transform (FFT) modulo q . All polynomials in the CKKS scheme are represented by default as a series of N evaluations at fixed roots of unity, allowing fast polynomial multiplications (in $O(N)$ time instead of $O(N^2)$). NTT is the finite field version of the fast Fourier transform (FFT) and takes $O(N \log N)$ time and $O(N)$ space for a degree- $(N - 1)$ polynomial. We call the output of the NTT on a polynomial its *evaluation representation*. If any operations are to be done over the polynomial's *coefficient representation*, then we need to perform an inverse NTT (iNTT) to move the polynomial back to its *coefficient representation*.

We would like to note that in addition to NTT polynomial transform the CKKS scheme also uses the FFT polynomial transform. On the client side, during CKKS encryption and decryption, a complex FFT must be run on vectors of complex numbers to map them to polynomials that can be encrypted. Correspondingly, on the cloud side, during bootstrapping, this complex FFT (which was performed on the client side) must be *homomorphically* evaluated on the encrypted data.

2.1.3 Bootstrapping

In order to compute indefinitely on a CKKS ciphertext, there needs to be an operation that raises the ciphertext modulus Q while maintaining the correct structure of the ciphertext. This operation is known as bootstrapping [10], and it is the main bottleneck for fully-homomorphic encryption. Optimizing bootstrapping is the main focus of FAB.

A detailed description of the bootstrapping algorithm is beyond the scope of this work. We refer the reader to [15] for a detailed description of the bootstrapping algorithm that we use. This analysis is particularly relevant for FAB because it optimizes for the memory bandwidth of the bootstrapping algorithm. Without this analysis and the resulting optimizations, FAB would also be bottlenecked by the memory bandwidth; however, with these optimizations, the memory bandwidth is no longer the bottleneck.

At a high level, the bootstrapping operation consists of three major steps: a linear transform, a polynomial evaluation, and finally another linear transform (inverse of the first step). All these steps consist of the same homomorphic operations described above (Add, Mult, Rotate, and Conjugate).

The polynomial evaluation is constrained by application parameters, and we use the same polynomial as Bossuat et al. [5] to support non-sparse CKKS secret keys. The multiplicative depth of this polynomial evaluation is 9.

The two linear transforms in bootstrapping are FFT and inverse FFT, which must be homomorphically evaluated on the encrypted data. There is a depth-performance trade-off in this algorithm that has been carefully studied in prior works [9, 25, 15]. This trade-off is parametrized by the chosen multiplicative depth of the FFT algorithm, which we denote as fftIter . A more detailed discussion of the effects of this parameter is given Section 2.2.

2.1.4 Bootstrapping Performance

We review the main performance metric that is used to evaluate the efficiency of bootstrapping, first introduced in [31]. After a bootstrapping operation, the resulting cipher-

text can support a certain number of computation levels ℓ before needing to be bootstrapped again. Since each level corresponds to a multiplication, the performance metric for a bootstrapping routine is as follows:

$$T_{\text{Mult},a/\text{slot}} := \frac{T_{\text{Boot}} + \sum_{i=1}^{\ell} T_{\text{Mult}}(i)}{\ell \cdot n} \quad (2)$$

This is known as the *amortized multiplication time per slot*. Here, n is the number of slots in the ciphertext, T_{Boot} is the bootstrapping time, and $T_{\text{Mult}}(i)$ is the time to multiply at level i .

The number of levels ℓ in the resulting ciphertext are equal to the maximum supported levels in the starting bootstrapping modulus minus the depth of bootstrapping. The depth of bootstrapping for our algorithm is $L_{\text{Boot}} := 2 \cdot \text{fftler} + 9$.

2.1.5 Switching Keys & Major Subroutines

The Mult, Rotate, and Conjugate operations all produce intermediate ciphertexts that are decryptable under a different secret key than the input ciphertext. These operations all use a common subroutine known as KeySwitch [8] to switch the decryption key back to the original value. KeySwitch represents a major bottleneck in low-level homomorphic operations.

All instances of KeySwitch require a *switching key*, which is a special type of key generated using the secret key but safe to publish along with the rest of the public key. The KeySwitch operation takes in a switching key $\text{ksk}_{s \rightarrow s'}$ and a ciphertext $[[\mathbf{m}]]_s$ decryptable under a secret key s and produces a ciphertext $[[\mathbf{m}]]_{s'}$ that encrypts the same message but can be decrypted under a different key s' . We use the structure of the switching key proposed by Han and Ki [27], where the switching key is parameterized by a length dnum and is a $2 \times \text{dnum}$ matrix of polynomials.

$$\text{ksk} = \begin{pmatrix} \mathbf{a}_1 & \mathbf{a}_2 & \dots & \mathbf{a}_{\text{dnum}} \\ \mathbf{b}_1 & \mathbf{b}_2 & \dots & \mathbf{b}_{\text{dnum}} \end{pmatrix} \quad (3)$$

We omit the descriptions of the CKKS subroutines. We use the same definitions as [15], and we refer the reader to [15] for a thorough description of these subroutines. For reference, we make use of the Decomp, ModUp, ModDown, KeySwitchInnerProd (which we call KSKIP), and Automorph subroutines.

During the course of key switching, the ciphertext coefficient modulus is raised from Q to $P \cdot Q$, where P is a fixed product of "extension limbs." The ciphertext modulus Q is split into at most dnum digits of equal size, and P must be larger than the largest product of the limbs in a single digit of Q . We refer the reader to [27] for more details, and we conclude by noting that the parameter $P \cdot Q$ is the maximum modulus for which security must be maintained.

2.2 Practical Parameter Set for FAB

To prototype an efficient FAB design on the Xilinx Alveo U280 FPGA, we identify an optimal FHE parameter set that can support CKKS bootstrapping as well as the computational requirement of a real-time machine learning application. The parameter N must be a power of two for efficiency

Table 2: Parameter set for FPGA implementation.

$\log q$	N	L	dnum	fftler	λ
54	2^{16}	23	3	4	128

of the NTT, and the largest power of two that still leaves the limbs small enough to fit in the on-chip memory is $N = 2^{16}$. Given this N , the maximum ciphertext modulus we can support is $\log(PQ) = 1728$, which achieves a 128-bit security level [3, 5]. These parameters also meet the constraints of our chip, since the maximum size of a single ciphertext is only 28.3 MB (based on the maximum number of raised limbs, which is 32 limbs). We can fit an entire ciphertext in the limited on-chip memory (43 MB) of our FPGA and thus limit the data movement to & from the main memory. Table 2 lists our choice of the other parameters based on the selected values for $\log(PQ)$ and N .

Limb Bit-Width. We fix the bit-width for each limb ($\log q$) as 54 bits for several reasons. First, a 54-bit limb width enables effective utilization of both the 18-bit multipliers and the 27-bit preadders within the DSP slices through multi-word arithmetic [28]. DSP slices have multipliers that are 18×27 -bit wide. Using multi-word arithmetic, we can split 54-bit operands into multiple 18-bit operands and operate over them in parallel. To perform integer additions, we split the 54-bit operands into two 27-bit operands to leverage the 27-bit preadders in the DSP blocks. Second, a 54-bit limb width allows us to make the most of the scarce on-chip memory resources, which includes both Ultra RAM (URAM) and Block-RAM (BRAM). On U280 cards, locations within a URAM block can store 72-bit wide data and locations within a BRAM block can store 18-bit wide data. Therefore, with 54-bit (a multiple of 18) coefficients in the vectors, we can effectively utilize the entire data width of the on-chip memory resources by combining multiple B/URAM blocks to store single/multiple coefficients at a given address. We discuss a detailed on-chip memory layout later in Section 4.

Higher-level Parameters. The dnum and fftler parameters directly impact a number of factors that determine the final amortized multiplication time per slot, including the bootstrapping runtime as well as the number of compute levels available after bootstrapping. Figure 1 shows that as we increase the dnum value, we add more compute levels after bootstrapping, but at the same time we increase the size of KeySwitch keys, further increasing the compute and on-chip memory requirements. At $\text{dnum} = 3$, we are able to make the best use of the on-chip memory for the corresponding KeySwitch key size.

As mentioned earlier in Section 2.1, bootstrapping performs an FFT and an inverse FFT as the first and last steps of the algorithm. There is a depth-performance trade-off between the chosen multiplicative depth of the FFT algorithm and the amount of compute required for the bootstrapping operation. This trade-off is parameterized by fftler , which is the multiplicative depth of the FFT algorithm. As the value of fftler increases, the multiplicative depth also increases implying fewer compute levels after bootstrapping. However, as we increase fftler , the radix of the FFT submatrices reduces, thus requiring fewer number of rotations

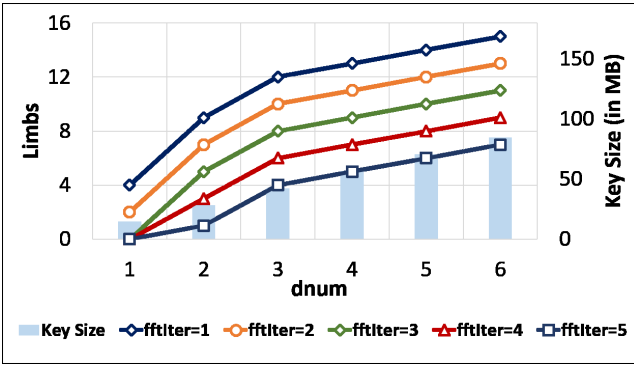


Figure 1: Impact of changing the $dnum$ parameter on the compute levels after bootstrapping and the switching key size. Note that we use the key-compression technique from [15] to halve the size of the keys.

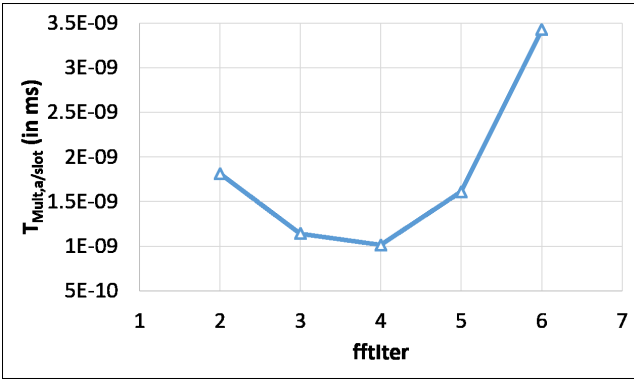


Figure 2: Effect of increasing $fftlter$ parameter on the execution time of bootstrapping. For all benchmarks we set $N = 2^{16}$, $\log(PQ) = 1728$, $\log(q) = 54$, and $dnum = 3$.

during each multiplication. Figure 2 shows how increasing the $fftlter$ parameter impacts the overall bootstrapping execution time and the number of NTT operations to be computed. The metric used to measure bootstrapping time is the amortized per slot multiplication time in equation 2. We pick $fftlter = 4$ as it generates an optimal balance between the computations (both rotations and NTTs) and the number of compute levels after bootstrapping. This fixes the total depth of our bootstrapping circuit as $L_{Boot} = 2 \cdot fftlter + 9 = 17$.

3. OVERALL SYSTEM ARCHITECTURE

In this section, we present the overall architecture (system view) that uses our proposed hardware accelerator. As shown in Figure 3, our overall system consists of four key components: a host CPU (X86 in our case) that offloads the RTL design and data to the FPGA, the RTL design that is packaged as a kernel code, global memory on the FPGA comprising of two HBM2 stacks (4 GB each), and a 100G Ethernet (CMAC) subsystem to enable transmit/receive data to/from FPGAs without involving the host.

On a cloud server, the host CPU is attached to an FPGA accelerator board (Alveo U280) via PCIe. This PCIe interface enables the data transfer between the host and the global memory on the FPGA board. To enable this data transfer, the host allocates a buffer of the dataset size in the global memory. The host code communicates the base address of the buffer with the kernel code using atomic register reads and writes through an AXI4-Lite interface. The host application also communicates all kernel arguments consisting of the system parameters like prime moduli, the degree of the polynomial modulus N , and the pre-computed scalar values (to be stored in the register file) through this interface. A kernel is started by the host code (written in native C++) using the Xilinx runtime (XRT) API call. It is worth noting that this XRT API call can be seamlessly replaced by an OpenCL [37] API call with trivial modifications to the host code. Once the kernel execution starts, no data transfer incurs between the host and the global memory so as to interface all 32 AXI ports from the HBM to the kernel code. The results are transferred back to the host code once the kernel execution completes.

The kernel code instantiates a functional unit consisting of 256 modular arithmetic and automorph units. A small register file (RF), 2 MB in size, stores all the required system parameters and the precomputed scalar values that are received from the host. The RF also facilitates temporary storage of up to four polynomials that may be generated as intermediate results. The kernel has 32 memory-mapped 256-bit interfaces that are implemented using AXI4 master interfaces to enable bi-directional data transfers to/from the global memory. The read (Rd) FIFO and write (Wr) FIFO stream the data from global memory onto the on-chip memory and vice-versa. The URAM and BRAM resources on the FPGA are organized into various banks to be used as on-chip memory within the kernel code. All of the URAM memory banks are single-port banks as URAMS do not support dual-port functionality, while the BRAM memory banks are dual-port banks. The transmit (Tx) and receive (Rx) FIFO stream the data to and from the CMAC subsystem.

The Alveo U280 FPGA has an integrated IP block for 100G Ethernet (CMAC) core, providing a high performance, low latency 100 Gb/s Ethernet port to transfer data between FPGAs that are connected to different hosts. The CMAC core has an internal clock operating at 322 MHz and the data interface with the kernel code can be either 256/512 bit wide. We implement a 512-bit interface in our kernel code to keep up with 100 Gbps transfer rates. This is because, with 512-bit interface at 300 MHz, we can theoretically process data at ~ 153 Gbps, which is faster than the Ethernet IP. However, with 256-bit interface, we can process data at ~ 76 Gbps, which is comparatively slower than the Ethernet IP and will end up dictating the final time it takes to transmit/receive the data to/from other FPGAs. Thus, with a 512-bit interface, it takes $\sim 11,399$ clock cycles to transmit a single limb of the ciphertext (polynomial of size 0.4 MB) and $\sim 546,980$ clock cycles to transmit the entire ciphertext.

4. FAB ARCHITECTURE

FAB consists of a functional unit, on-chip memory (URAM

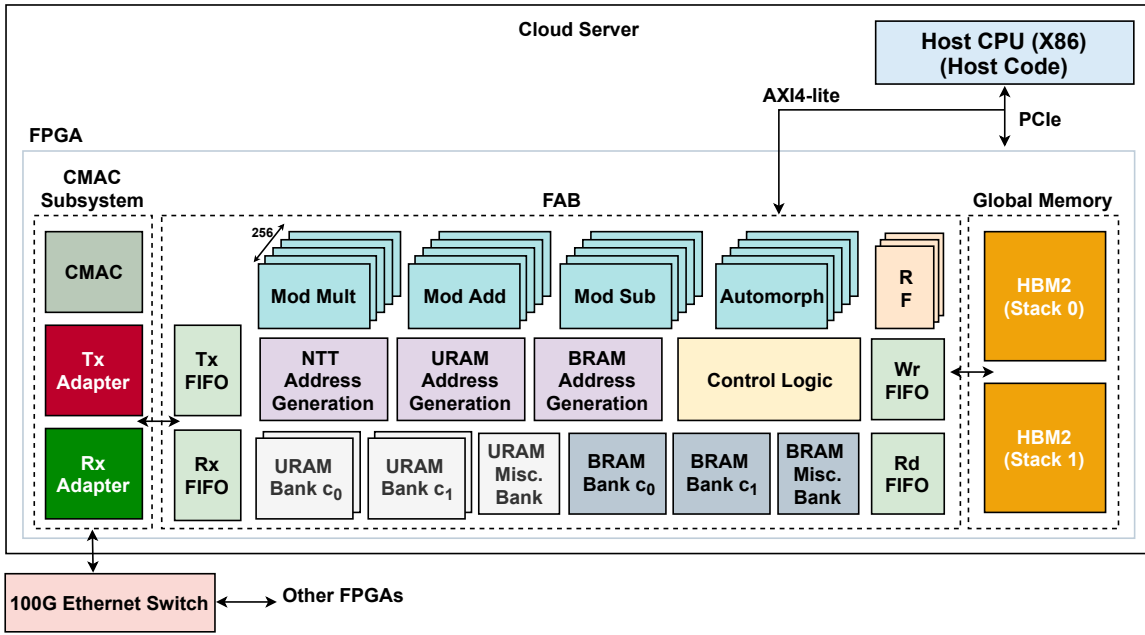


Figure 3: An FPGA-based system consisting of a host CPU, FPGA programmable logic, HBM2 memory and CMAC system for FHE-based computing. We map our FAB accelerator to the FPGA programmable logic. The host CPU interacts with the FPGA via PCIe. CMAC subsystem enables interaction between multiple FPGAs via Ethernet Switch.

and BRAM), register file (RF), FIFOs, address generation units, and control logic. In this section, we discuss the microarchitecture of each of these units. These units are architected so as to achieve a balanced full-system design.

4.1 Functional Unit

All operations in FHE break down to integer modular arithmetic i.e., modular addition and modular multiplication operations. Therefore, each of the 256 functional units in FAB consists of a modular multiplication, modular addition, modular subtraction, and an automorph unit. As mentioned in Section 2.2, we utilize a multi-word arithmetic approach to reduce 54-bit operations to 27-bit operations for addition and 18-bit operations for multiplication. This facilitates efficient utilization of specialized DSP arithmetic blocks on the FPGA.

For multi-word modular addition and subtraction, we follow Algorithms 2.7 and 2.8 proposed by Hankerson et al. [28], respectively. Both of these algorithms (on line 2 in Algorithms 2.7 and 2.8) require a correction step for modular reduction, which leads to 54-bit addition/subtraction operations again. Subsequently, we modify the correction step in both the algorithms to perform multiple 27-bit operations instead. With multi-word arithmetic and all the pipeline registers in place for the DSP blocks, both algorithms perform modular addition and subtraction in 7 clock cycles.

The modular multiplication is accomplished by first multiplying the operands as integers, and then reducing the result. This implies that the modular multiplication is split across two operations i.e., an integer multiplication followed by a modular reduction in a pipelined fashion. For the in-

Algorithm 1 Modular Reduction in \mathbb{F}_q

- 1: Modulus q , integer a , $shifts = 6 \triangleright a$ is $(2 \log q - 1)$ bits
 - 2: Precompute: $madd[i - 1] = \sum_{j=0}^5 i[j] \cdot 2^{\log q + j} \pmod{q}$
for $i = 1$ to $2^{shifts} - 1 \triangleright madd$ has $\log q$ -bit elements
 - 3: Set $(A[1], A[0]) \leftarrow a$, $count = 0$, $as_1 = 0$
 - 4: **while** $count < \log q$ **do**
 - 5: $(carry, as_1) = A[1] \ll shifts \triangleright carry$ is $shifts$ bit
 - 6: $A[1] = as_1 + madd[carry - 1]$
 - 7: $count = count + shifts$
 - 8: **end while**
 - 9: $c = A[1] + A[0]$
 - 10: **if** $c > q$ **then**
 - 11: $c = c - q$
 - 12: **end if**
 - 13: **return** c
-

teger multiplication, we follow the operand scanning algorithm [28] (algorithm 2.9) that adopts the schoolbook approach to perform multi-word multiplication. As we split our input 54-bit operands into three 18-bit operands, a naïve implementation of this algorithm will require 21 clock cycles to perform a single multiplication. Given the fact that most FHE workloads have 50% of the operations as integer multiplication, a latency of 21 clock cycles for a single integer multiplication is too high. Consequently, we perform loop unrolling on this algorithm and compute various operations in parallel, reducing the multiplication latency to 12 clock cycles while still adding all the required pipeline registers for DSP multipliers.

For modular reduction, we propose a hardware-friendly

fast modular reduction algorithm by modifying Will and Ko’s reduction technique [44]. As opposed to standard modular reduction approaches like Barrett reduction [4], which requires performing multiple expensive multiplication operations, Will and Ko’s technique requires only shift and addition operations. It works by shifting a single bit of the input number, making it a good choice for inputs with smaller bit widths. For our $(2 \log q - 1)$ -bit wide number, Will and Ko’s technique takes $2 \log q$ cycles (for $\log q = 54$ it takes 108 cycles) to compute a modular reduction. To reduce this latency while leveraging the simplicity of their approach, we propose Algorithm 1 that can instead perform multiple bit shifts at a time requiring only 12 clock cycles for $\log q = 54$ for the modular reduction operation. We set the number of shifts to 6 (line 1 in Algorithm 1) in our implementation, but it is worth noting that this algorithm is generic and can work with any number of bit shifts depending on the latency requirement and space constraints. This algorithm requires precomputing an array `madd` (line 2 in Algorithm 1) having 63 elements, where each element is $\log q$ -bit wide. In our case, we need to perform modular reduction w.r.t 32 different prime moduli, implying that we will need to precompute 32 such `madd` arrays requiring 7 KB of storage space in total. However, this precompute is done offline, so there is no compute overhead associated with it. All the other steps in the proposed algorithm are straightforward and can be performed using inexpensive shift and addition operations.

The final operation that forms part of the functional unit is Automorph, which performs permutation for the Rotate operation. The function of the automorph unit is to read a polynomial from the on-chip memory and store it in the register file in the permuted order as per the given rotation index k . Any original slot indexed by i in a ciphertext maps to the rotated slot through the given automorphism equation:

$$\text{new_index}_k(i) = \frac{5^k - 1}{2} + 5 \cdot i \pmod{N} \quad (4)$$

Due to the limited number of rotation indices (about 60 different values) being used in bootstrapping, we precompute and store the various powers of 5 corresponding to each of the rotation index k . The division by two is a simple bit-shift, and the reduction modulo N is significantly simplified because N is always a power of two. Thus, reduction modulo N can be achieved by simply performing the AND operation with $N - 1$.

Summary. To summarize, the functional units in FAB are highly optimized for hardware to incur less resource overhead. They make effective use of high-performance multipliers and adders in DSP blocks to perform low latency modular arithmetic. FAB efficiently utilizes these functional units through fine grained pipelining and by issuing multiple scalar operations in a single cycle.

4.2 On-chip Memory

The Alveo U280 accelerator board has single-cycle access URAM and BRAM blocks. There are 962 blocks of URAM where each block is 288 Kb and can be used as single-port memory. There are 4032 blocks of BRAM where each block is 18 Kb and can be used as both single and dual-port mem-

ory. FAB uses a combination of single and dual-port memory banks constructed using URAM and BRAM blocks, providing a total capacity of 43 MB and a 30 TB/s internal SRAM bandwidth.

As shown in Figure 4 (a), each URAM block has data width of 72-bits and a depth of 4096. We combine three such URAM blocks to achieve a data width of 216-bits. This allows us to store four 54-bit coefficients ($216/4 = 54$) at any given address. Consequently, we need to layout 64 of these 216-bit wide URAMs into a single memory bank to enable storage of 256 coefficients. Thus, with every read and write, we can access 256 coefficients in the same cycle, aligning with the number of functional units in the design. With this layout, a single memory bank consists of $64 \times 3 = 192$ URAMs and can store 16 polynomials (~ 7.08 MB). We organize the available URAM blocks into five such banks that are divided as follows: The first two banks (c_0 bank-1 and 2) store 32 limbs (24 original and 8 extension) of the c_0 ring element of the ciphertext. The next two banks (c_1 bank-1 and 2) store 32 limbs (24 original and 8 extension) of the c_1 ring element of the ciphertext. The fifth bank can store 16 polynomials. We call the fifth bank the "miscellaneous" bank as it is used to store multiple data items such as twiddle factors, KeySwitch keys, and plaintext vectors that are read in from the main memory.

As shown in Figure 4 (b), BRAM blocks are organized as 54-bit wide memory banks by combining three 18-bit wide BRAMs. Since each address can store only a single 54-bit coefficient, we need 256 BRAM blocks to store 256 coefficients. In addition, the depth of each BRAM block is only 1024; therefore, we stack two BRAM blocks to get a depth of 2048, thus enabling storage of 8 polynomials in a single BRAM bank. Similar to URAM bank organization, we organize BRAM blocks into multiple banks. We have three BRAM banks in total, where two banks consists of 1536 BRAMs each and can store 8 polynomials and thus, are ideal to store the extension limbs. While the third bank consists of 768 BRAMs and can store 4 polynomials. We again call this third bank the "miscellaneous" bank and use it to store temporary data from main memory during various operations.

Summary. To summarize, FAB architecture efficiently utilizes the available U/BRAM blocks on the FPGA as on-chip memory. Mapping the polynomial data bit-width to that of the U/BRAM blocks data width enables storage of up to 43 MB of on-chip data. FAB overcomes the limited main memory bandwidth issue by utilizing a combination of single and dual-port memory banks that complement the operational needs of the underlying FHE operations, resulting into a more balanced FPGA design.

4.3 Register File

Our design consists of multiple register files (RFs). The total capacity of all the register files is 2 MB. The register files are spread across the design and are used by functional, address generation and control units. Each RF has multiple read/write ports with same cycle access latency. About one-fourth of the register file is used to store pre-computed values and system parameters, which are written by the host CPU through atomic writes before launching the kernel code

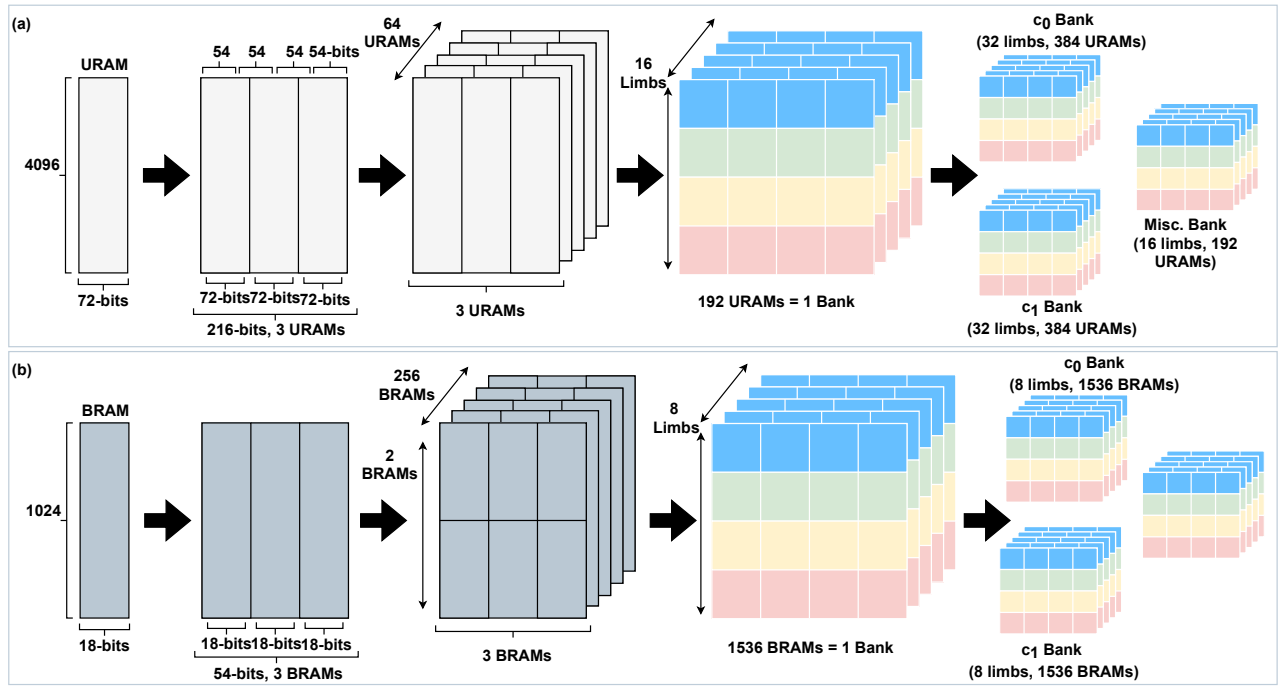


Figure 4: On-chip memory configuration; (a) URAM blocks are organized into five different memory banks and (b) BRAM blocks are organized as three different memory banks.

execution. The remaining RFs are used to store up to four intermediate polynomials that are generated as part of Rotate or Mult operations.

4.4 FIFOs

We instantiate 32 synchronous Write (Wr) and Read (Rd) FIFOs (supporting 32 AXI ports on the HBM-side) to stream the data between the main memory and the on-chip memory. These FIFOs are composed of the distributed RAM available on the FPGA board. The data width of each FIFO is equal to the data width supported by each AXI port i.e., 256-bits. The depth of the Wr FIFO is 128 to support an HBM burst length of 128. The depth of the Rd FIFO is 512 to support up to four outstanding reads. Rd FIFO is driven by the memory-side clock domain having a clock frequency of 450 MHz while the Wr FIFO is driven by the kernel-side clock domain having a clock frequency of 300 MHz. We also instantiate a Transmit (Tx) and Receive (Rx) FIFO to stream the data between the CMAC subsystem and the on-chip memory. These are also synchronous FIFOs having a 512-bit data interface.

4.5 NTT/iNTT datapath

Our NTT datapath uses a unified Cooley-Tukey algorithm [38] for both NTT and inverse-NTT (iNTT). Using a unified NTT algorithm provides the convenience of leveraging the same data mapping logic for both NTT and iNTT. The 256 modular addition, subtraction and multiplication units operate in parallel as radix-2 butterfly units, processing 512

coefficients of a polynomial at once. This allows us to perform $\log N$ stages in approximately $\log N \cdot \frac{N}{512}$ cycles instead of $\log N \cdot \frac{N}{2}$ cycles. The NTT address generation unit (shown in Figure 3) takes care of uniquely mapping the data within each stage of the NTT/iNTT using a sub-unit, i.e. a data mapping unit. Furthermore, a twiddle factor mapping sub-unit within the NTT address generation unit takes care of reading the required twiddle factors for an NTT stage from the URAM miscellaneous bank. Both of these sub-units leverage the data and stage counters to generate the addresses on-the-fly using inexpensive shift, and AND operations. Thus, we efficiently leverage pipelining and parallelism while computing NTT/iNTT by spreading the computations over the functional units, a data mapping unit, and a twiddle factor mapping unit. It is worth noting that we do not take into account the latency of the bit-reversal operation here as bit-reversal is carried out along with automorph/multiplication operation that is performed just before NTT/iNTT.

4.6 Key Switch datapath

A KeySwitch operation comprises of four sub-operations, i.e., Decom, ModUp, KSKIP, and ModDown. With limited on-chip memory, these operations require smart operation scheduling to efficiently utilize the on-chip memory. This is because KeySwitch not only needs to operate on the extension limbs (the factors of P) but it also needs to perform inner product with the KeySwitch keys that are almost three times the size of our ciphertext. **Below we present a detailed description on how we schedule and reorganize the sub-operations in KeySwitch to manage ~ 112 MB of**

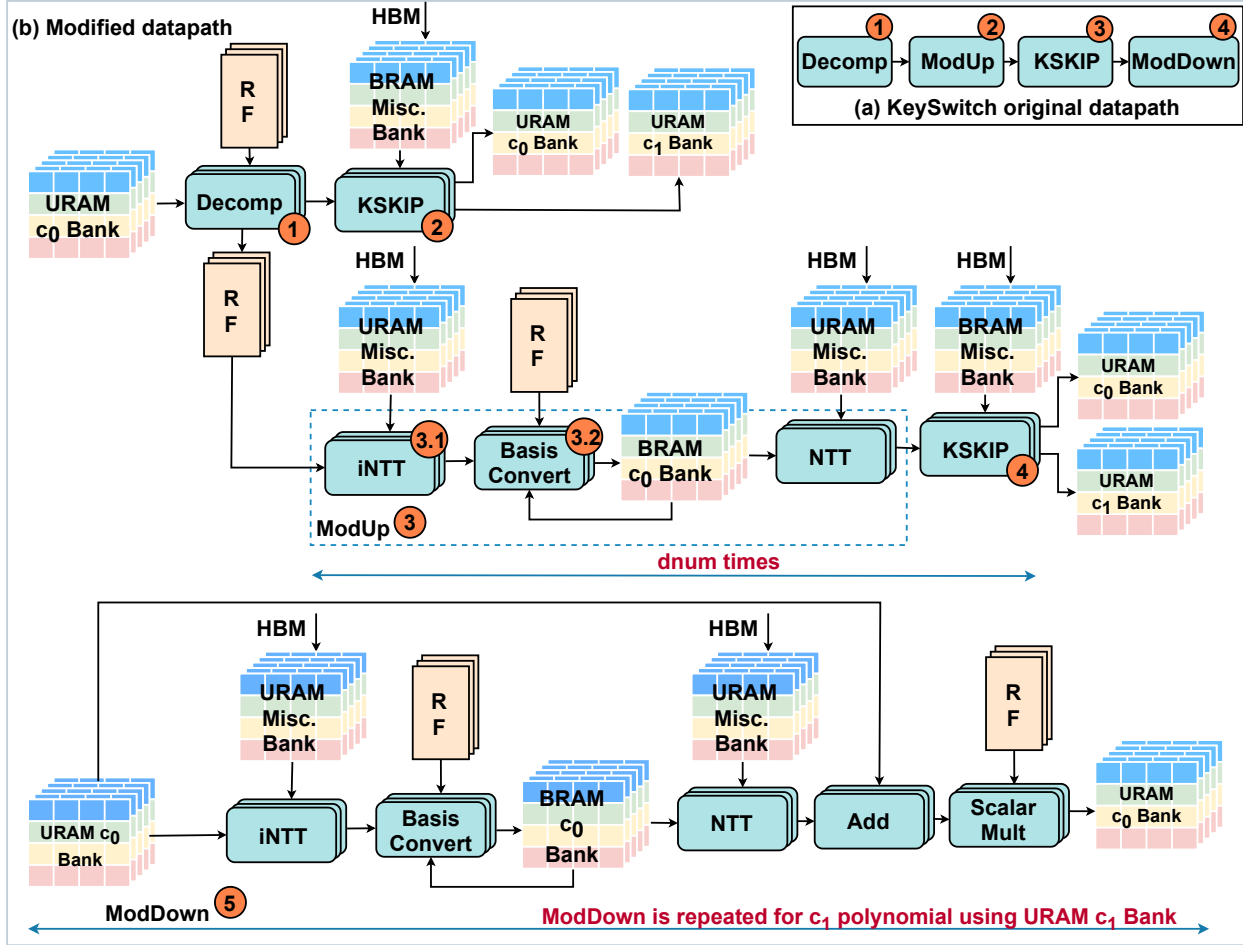


Figure 5: (a) Original datapath. (b) Modified datapath for efficient on-chip memory utilization for the four main operations (Decomp, ModUp, KSKIP, and ModDown) within the KeySwitch Operation. Our approach avoids reads/writes of the ciphertext limbs to the main memory, which lowers the latency of FHE-based computing.

data (84 MB keys and 28 MB ciphertext) within the available 43 MB on-chip memory without the need of writing any resultant limbs back to the main memory.

The Decomp sub-operation splits the limbs in \mathbf{a}_m ring element (ciphertext has two ring elements \mathbf{a}_m and \mathbf{b}_m) into $dnum$ digits. Each of these digits is then passed into ModUp. ModUp outputs $L + 1 + \alpha$ limbs; after all ModUp operations are complete we have $dnum \cdot (L + 1 + \alpha)$ limbs in total. In our case, $dnum = 3$ and $\alpha = 8$. This results in $3 \cdot 32 = 96$ total limbs after all instances of the ModUp operation have finished. Therefore, to manage all 96 limbs in on-chip memory (without having to write any resultant limb back to main memory), we modify the KeySwitch datapath to reorganize the execution of sub-operations in KeySwitch. Naïvely, one would execute the sub-operations one after another following the original datapath as shown in Figure 5 (a). However, there are challenges associated with this approach that FAB addresses through the modified datapath (refer Figure 5 (b)) and smart operation scheduling.

Modified datapath: We modify the original KeySwitch datapath so as to split the KSKIP step into two steps. Rather

than perform the KSKIP step all at once, we "greedily" make progress on the inner product by performing the multiplications and additions as soon as the operands are in memory, which saves DRAM transfers.

In more detail, the KSKIP step is an inner product between the input polynomial and the switching key in the raised basis. In the original KeySwitch data path, the full ModUp step is performed to extend the RNS basis of the input polynomial, then the full KSKIP is performed. There is not enough space in the on-chip memory to hold all the extended polynomials, and so the original datapath first reads in the input limbs in evaluation representation to perform the Decomp step, then writes the limbs out in coefficient representation after the ModUp step. These limbs are then read back into the chip memory to perform the KSKIP step.

This optimization identifies that α limbs in each ModUp operation do not change, so we can use these limbs to immediately begin the KSKIP step once the Decomp step is finished. More specifically, the Decomp step takes these L limbs and splits them into $\beta \leq dnum$ blocks of α limbs each. These α limbs then take two paths. First, these α limbs are

used to begin the KSKIP, and the intermediate sum is written out to URAM. The second path these α limbs take is as input to the basis conversion step so that the extension limbs can be generated. Once these extension limbs are generated, they are used to complete the KSKIP step. **Thus, the modified datapath not only reduces the number of NTT computations (the most expensive subroutine in KeySwitch operation) but also helps alleviate the memory bandwidth bottleneck by reducing memory traffic.**

Smart operation scheduling: Smart operation scheduling takes advantage of a straightforward optimization in the RNS extension equation in Equation (1). Naively, for each new limb p_j that must be generated, we must perform 2ℓ multiplications. However, we can observe that one of the multiplications (specifically the $x_i \cdot \tilde{Q}_i$ product) is not dependent on the output modulus. Therefore, we can compute the ℓ inner multiplications of the form $x_i \cdot \tilde{Q}_i \pmod{q_i}$ and then reuse these products when computing all of the extension limbs p_j . This reduces the number of modular multiplications by a factor of two.

Smart operation scheduling also complements the modified datapath by generating an entire block of extension limbs at once for the given the original α limbs. As soon as all of the extension limbs for one block of α limbs is computed, we perform an NTT followed by KSKIP on these limbs before generating the next block of extension limbs. This process is repeated $dnum$ times to generate all $dnum \cdot (L + 1 + \alpha)$ limbs. Note that we do not need to fetch all the KeySwitch keys at once; we only need to fetch the block of the key corresponding to the α block that has just been extended. Moreover, all extension limbs are always stored in c_0 BRAM bank because the dual-port BRAMs supplement BasisConvert operation by allowing data reads and writes at the same time to perform inner products in *limb-wise* fashion. Through these methods, we perform the entire KSKIP using a small BRAM miscellaneous bank (that can store only 4 limbs), while hiding the key read latency (which is about 300 clock cycles) from the main memory behind the computations. The ModDown (step-5 in Figure 5 (b)) operation follows a similar operation scheduling as ModUp operation. **Thus, through smart scheduling we enable high data reuse, exploit inherent limb-wise parallelism and maintain a uniform address generation logic by avoiding to switch between limb-wise and slot-wise accesses, and further reduce the main memory traffic by not writing/reading any resultant ciphertext limbs to the main memory.**

We would like to mention that the split of the KSKIP into two steps does not change the underlying KeySwitch algorithm, only the order in which the steps are performed changes. The resulting noise from the KeySwitch algorithm is identical with or without this reordering. Although our KeySwitch datapath optimization is specific to Alveo U280 FPGA, it can be ported to smaller FPGAs as long as one can accommodate at least one limb of the key and the ciphertext polynomial in on-chip memory. If not, then some additional fine grain optimizations will have to be developed such as changing the BasisConvert operation to perform all operations *slot-wise* instead of *limb-wise*. This is to efficiently manage reading the slots from within a key limb so that the problem does not become memory bound.

Table 3: FAB Hardware Resource Utilization

Resource	Available	Utilized	% Utilization
LUTs	1,304K	899,232	68.96
FFs	2,607K	2,073K	79.54
DSP	9,024	5,120	56.70
BRAM	4,032	3,840	95.24
URAM	962	960	99.80

Table 4: Comparison of modular multiplier count, register file size and on-chip memory size in different designs.

Work	Parameters ($N, \log q$)	Modular multipliers	Register file (MB)	On-chip memory (MB)
F1 [41]	$2^{14}, 32$	18432	8	64
BTS [35]	$2^{17}, 50$	8192	22	512
FAB	$2^{16}, 54$	256	2	43

5. EVALUATION

5.1 Setup

We designed FAB in Verilog 2001 and synthesized it using Xilinx Vivado 2020.2 to operate at 300 MHz frequency. The host CPU code is written in C++. FAB RTL code is packaged into kernel code using the Xilinx Vitis 2020.2 development platform. The kernel code is compiled and linked into an FPGA executable (.xclbin binary file) by the Vitis compiler. In the cloud environment, this binary file is mapped to a Xilinx Alveo U280 FPGA and its execution is initiated by the host CPU via host code. This accelerator FPGA card is built on the Xilinx 16nm UltraScale architecture and offers 8 GB of HBM2 with up to 460 GB/s bandwidth.

5.2 Resource Utilization

Table 3 provides the hardware resource utilization of the various components of FAB. Overall, FAB requires $\sim 899K$ LUTs, and the functional units represent the largest share ($\sim 37\%$) of these LUTs. The remaining utilization is among the control unit, the various address generation units and the FIFOs. Out of the 2,073K flip flops (FFs) used by FAB, most of them are utilized by the distributed register file, control logic and the functional unit. The entire 56.7% of the DSP utilization is for the modular arithmetic operations within the functional units. As mentioned earlier in Section 4.2, FAB makes use of almost the entire URAM and BRAM blocks on FPGA; we observe a 95.24% BRAM utilization and 99.8% URAM utilization.

5.3 Comparison of Basic FHE Operations

Table 5 presents the execution time (in ms) for basic operations in the CKKS FHE scheme and compares the performance with the existing GPU implementation [31]. The GPU numbers used in the table are the most optimized performance numbers reported by the authors for the parameter

Table 5: Execution time (in ms) for performing basic CKKS FHE operations and speedup achieved using FAB.

Operation	FAB	GPU	Speedup vs GPU
Add	0.04	0.16	$3.85\times$
Mult	1.71	2.96	$1.73\times$
Rescale	0.19	0.49	$2.62\times$
Rotate	1.57	2.55	$1.62\times$

Table 6: Throughput (in operations per second) comparison for basic operations with HEAX. Throughput numbers reported here are for $N = 2^{14}$ and $\log Q = 438$.

Operation	FAB	HEAX	Speedup vs HEAX
NTT	167K	42K	$3.97\times$
Mult	5.7K	2.6K	$2.12\times$

set $N = 2^{16}$, $\log Q = 1693$, and 100b security. We compare against these numbers as the parameter set is closest to our parameters. FAB achieves an average $2.4\times$ speedup when compared to GPU in absolute execution time for these basic primitives. For completeness, in Table 6, we compare the performance of NTT and Mult with an existing state-of-the-art FPGA implementation (HEAX [39]). For a fair comparison, we use the same parameter set ($N = 2^{14}$ and $\log Q = 438$) as used in HEAX. FAB achieves an average $3\times$ higher throughput (in operations per second) when compared to HEAX. The performance gain in FAB is largely due to low latency modular arithmetic modules within functional units, fine-grained pipelined usage of the functional units, highly optimized NTT datapath, and the modified KeySwitch datapath.

We do not compare FAB against ASIC implementations of CKKS such as F1 [41] that do not support parameters large enough for fully-packed bootstrapping. Also note that several works [5, 35] do not give low-level benchmarks for the individual homomorphic operation. For these works, we compare against the amortized multiplication time in Table 7.

5.4 Bootstrapping Latency

As described earlier, the bootstrapping operation is the key bottleneck for performing unbounded FHE computations. In this section, we compare the bootstrapping latency of FAB with the existing state-of-the-art CPU, GPU, and ASIC implementations. Throughout this section, we refer to these implementations as Lattigo [5] (CPU implementation), GPU-1 for 97-bit security and GPU-2 for 173-bit security (GPU implementations of [31]), F1 [41], and BTS-2 [35] (ASIC implementations). Following the bootstrapping performance metric from these existing works, we compare against these works using the amortized per slot multiplication time $T_{Mult,a/slot}$ defined in equation 2.

As seen in Table 7, FAB outperforms CPU, GPU-1, GPU-2 and F1 implementations in absolute time. This is despite the lower operating frequency of FAB, and when comparing the clock cycles against prior works FAB compares even more favorably. FAB exhibits a better performance due to improved arithmetic intensity by overcoming memory band-

Table 7: Speedup achieved using FAB when performing bootstrapping operations. Slots define the number of packed slots in the ciphertext while bootstrapping. Bootstrapping time is computed in $T_{mult,a/slot}$.

Work	Freq. (in GHz)	Slots	Time (in μs)	Speedup achieved using FAB (Time)	Speedup achieved using FAB (Cycles)
Lattigo	3.5	2^{15}	101.78	$213\times$	$2485\times$
GPU-1	1.2	2^{15}	0.740	$1.55\times$	$6.35\times$
GPU-2	1.2	2^{16}	0.716	$1.50\times$	$6.14\times$
F1	1	1	254.46	$533\times$	$1775\times$
BTS-2	1.2	2^{16}	0.0455	$0.09\times$	$0.38\times$
FAB	0.3	2^{15}	0.477	-	-

width bottleneck. However, FAB is about $9\times$ (absolute time) and $4\times$ (clock cycles) slower than the best case numbers reported by BTS (i.e., for BTS-2). This difference in performance is mainly because of the large on-chip memory and a large number of modular multipliers used for computation in BTS when compared to FAB.

In Table 4 we highlight the difference in the resources utilized by the ASIC implementations and FAB to achieve the aforementioned performance. We perform this comparison in terms of the number of modular multipliers (MMs) used, the size of the register file and the on-chip memory. When compared to BTS, FAB requires $32\times$ less MMs, $11\times$ smaller register file and $12\times$ smaller on-chip memory. Moreover, the BTS design uses an ASAP7 technology node leading to an expensive design (in terms of fabrication cost and engineering design team cost). In contrast, we use FPGAs that are available today and our solution can be readily deployed in today’s cloud systems. If FAB were to implement 8192 MMs and a 512 MB on-chip memory, FAB will be at least $3\times$ faster than BTS owing to its optimization to the bootstrapping algorithm and the microarchitecture implementation.

5.5 Logistic Regression (LR) Training

In this section, we evaluate the use of FAB to perform LR model training for binary classification over a subset of MNIST data [16] labeled 3 and 8. This is the task considered in the HELR work [26], and it is the same task used to benchmark all works we compare against.

This subset of the dataset contains 11,982 training samples where each sample has 196 features. The LR model is trained for 30 iterations with 1024 encrypted images in a mini-batch. We adopt the sequence of operations proposed by Han et al. [26] for efficient logistic regression training on encrypted data. Using this algorithm, LR training for 30 iterations has an evaluation depth of 150, and thus, it requires us to perform a bootstrapping operation after every iteration.

We perform training using sparsely-packed ciphertexts (using 256 slots only). This is largely to perform a fair comparison with existing works (GPU-2 and BTS-2) that have only considered sparsely-packed ciphertexts (256 slots) for LR training. This is because 256 slots is optimal for the spe-

cific benchmark task, but our LR training implementation can easily scale to larger applications (i.e. applications that require fully-packed bootstrapping).

To evaluate LR training, we present two different FPGA designs here; 1) FAB-1: a single-FPGA design and 2) FAB-2: a multi-FPGA design that utilizes eight FPGAs. Note that FAB-2 will incur eight times the resource utilization as FAB-1. We follow the data partitioning and packing technique proposed in Han et al. [26] to pack the data efficiently into ciphertexts. Our FAB-1 design is a straightforward mapping of FAB onto an Alveo U280 board with all the ciphertexts and KeySwitch keys (~ 6.65 GB data) offloaded to the HBM2 of the FPGA. For the FAB-2 design, we instantiate FAB on all eight FPGA boards in the cloud environment, where each FPGA is connected to a host CPU. We form FPGA pairs, and in each pair, we designate a primary FPGA and a secondary FPGA to enable point-to-point communication between the FPGAs. In addition, one of the eight FPGAs acts as a master FPGA that can broadcast a ciphertext to the entire pool of FPGAs. We limit the impact of network communication on the performance of our FAB-2 design by using direct network communication between the FPGAs instead of involving the host CPUs. All the host CPUs launch the required kernel code on their respective FPGAs in parallel, which allows multiple ciphertexts to be processed in parallel. Since the ciphertexts are sparsely-packed, each FPGA needs to compute on 128 ciphertexts. Communication between the FPGAs needs to happen only twice during the execution of an entire LR iteration. This communication overhead is about 12ms per LR iteration.

Table 8 presents the average training time per LR iteration. In terms of absolute execution times, FAB-2 is $456\times$ and $9.5\times$ faster than existing state-of-the-art CPU and GPU implementations (for parameter set having $N = 2^{17}$ and $\log Q = 2395$). FAB-2 is even faster when we compare the speedup in terms of clock cycles. When comparing to ASIC proposals, FAB-2 outperforms F1 by $12\times$ while achieving a competitive performance when compared to BTS-2. Compared to FAB-1, FAB-2 (using eight FPGAs) does not observe a corresponding $8\times$ speedup as the amount of parallelism that can be extracted is limited by the bootstrapping runtime (following Amdahl’s law). This is because FAB is designed to perform bootstrapping on a single FPGA, so the performance increase is due to parallelizing the other operations within a logistic regression iteration. In principle, it is possible to improve the performance of FAB-2 by scaling bootstrapping operation to multiple FPGAs by exploiting instruction level parallelism. However, this requires distributing the operations (on a single ciphertext) to multiple FPGAs while minimizing data hazards and managing the large communication overhead. This is part of our future work.

Comparison with Leveled FHE Approach: Here we briefly compare our bootstrapping-based FHE approach against the leveled FHE approach. The leveled FHE approach avoids bootstrapping by simply having the cloud host send a ciphertext with no remaining compute levels back to the client, who holds the decryption key. The client then decrypts the ciphertext and re-encrypts the resulting message into a new ciphertext with some fixed number of compute levels. This new ciphertext is sent back to the cloud host to proceed with

Table 8: Performance comparison for LR training when using sparsely-packed ciphertexts [35]. Time reported here is average training time per iteration.

Work	Time (in sec)	Speedup achieved using FAB-2 (Time)	Speedup achieved using FAB-2 (Cycles)
Lattigo	37.05	$456\times$	$5318\times$
GPU-2	0.775	$9.5\times$	$39\times$
F1	1.024	$12\times$	$41\times$
BTS-2	0.028	$0.3\times$	$1.4\times$
FAB-1	0.103	$1.3\times$	$1.3\times$
FAB-2	0.081	-	-

the homomorphic computation.

There are several drawbacks to this approach. The most immediate is information leakage, which could make this approach completely unusable in some applications. This leakage is due to the intermediate values of the computation being revealed to the client; in contrast, only the final output value is revealed to the client when bootstrapping is run on the cloud machine. In order to defend against this leakage, the cloud host will need to add a λ -bit mask to the plaintext in order to achieve λ bits of security. This is because the CKKS plaintext space is *not* finite¹. In order to maintain correctness, this requires the CKKS plaintext to support an additional λ bits beyond the original plaintext value. The minimum λ that could be justified is $\lambda = 40$, which would require a significant increase in the CKKS parameters and result in a significant increase in the LR training time.

Even if we ignore the information leakage, FAB still outperforms the leveled FHE approach. A single iteration of logistic regression consumes 5 compute levels and requires bootstrapping at the end of each iteration. Using FAB, one iteration takes 0.103 seconds, which includes the bootstrapping time. For the leveled FHE approach, the encryption on the client side itself (using the sub-routines in the SEAL library) takes 0.162 seconds with a 2.8 GHz CPU. Adding the time for operations in the cloud and the time for client-cloud communication further increases the time per LR iteration.

6. RELATED WORK

CPU/GPU-based Acceleration: Many software libraries such as SEAL [42], HELib [29, 23], PALISADE [43], Lattigo [36], and HEAAN [33] implement the CKKS scheme on CPU. Despite the efforts of these libraries, a pure-CPU implementation of FHE remains impractical. A number of works [34, 45, 21] focus on accelerating just the NTT computation on a GPU. The current state-of-the-art for pure-CPU/GPU implementation of the full suite of FHE (including basic operations and bootstrapping) is the work of Jung et al. [31] which proposed the first GPU-accelerated implementation of the CKKS scheme.

ASIC-based Acceleration: Samardzic et al. [41] present the F1 hardware accelerator architecture for FHE computations.

¹This is in contrast to FHE scheme such as BGV [7] and BFV [6, 18], which have finite plaintext spaces. For these schemes, a uniformly random mask can be added to hide the message without requiring any additional bits of precision.

Although the accelerator supports multiple FHE schemes including BGV [20], CKKS, and GSW [30], it only supports operations on smaller parameter sets. To support multi-slot bootstrapping and the larger applications that require multi-slot bootstrapping (e.g. real-time machine learning), larger parameters are required, making the F1 chip incompatible with these applications. Kim et al. [35] proposed the BTS accelerator specifically tailored to efficiently support CKKS bootstrapping. BTS employs a massive number of processing elements to exploit parallelism in various homomorphic operations and makes use of large on-chip memory with a large register file. Despite these resources, they do not modify the underlying algorithm to fully optimize for the memory bandwidth. This results in unrealized performance when compared to the resources they use.

FPGA-based Acceleration: FPGAs are a more suitable candidate for high-performance and low-power secure computation. HEAX [39] is an FPGA-based accelerator that accelerates only CKKS encrypted multiplication. Other operations are deferred to a host processor. Moreover, this FPGA implementation supports only smaller parameter sets that allow computation up to multiplicative depth 10, which is not sufficient for bootstrapping or applications such as logistic regression training. Given these limitations, it is unclear how to implement a full-scale CKKS FHE workload and an end-to-end application on an FPGA. In our work, we implement the full-scale CKKS FHE bootstrapping, and we do so with secure parameter sets that support end-to-end applications. We evaluate a full system for secure logistic regression on an FPGA.

Applicability to Other Schemes: Although FAB implements the CKKS scheme-specific bootstrapping, our implementations of the basic operations such as Add, Mult, and Rotate that are common across schemes can be used for the BGV [7] and B/FV [6, 18] schemes. FHE schemes like TFHE [13] and FHEW [17] evaluate Boolean gates on encrypted data while incurring several GB memory footprint for encrypted keys [22]. Even for these schemes optimizations similar to KeySwitch datapath and smart operation scheduling are very relevant. However, the specific steps within the KeySwitch operation for all of these other schemes differ from those in the CKKS scheme, and so a thorough analysis is required to determine the exact operation scheduling so as to develop a balanced FPGA design.

7. CONCLUSION

We propose FAB, an FPGA-based accelerator for bootstrappable FHE. FAB leverages a combination of algorithmic and architectural optimizations to overcome the memory bandwidth bottleneck and to perform the first ever fully-packed bootstrapping on FPGA for a practical parameter set. Through smart operation scheduling and memory management techniques, FAB efficiently utilizes the limited compute and memory resources on the FPGA to deliver $456\times$ and $6.5\times$ better performance than CPU and GPU, respectively, for LR training application. More importantly, for the same LR training application FAB uses only currently-existing hardware while delivering performance comparable to the specialized and costly ASIC designs for bootstrap-

table FHE. FAB is also immediately accessible to the general public as all the resources required to support FAB exist in public commercial cloud environments.

REFERENCES

- [1] C. Aguilar-Melchor, “Nflib: Ntt-based fast lattice library,” in *Cryptographers’ Track at the RSA Conference*. Springer, 2016, pp. 341–356.
- [2] A. Al Badawi, B. Veeravalli, C. F. Mun, and K. M. M. Aung, “High-performance fv somewhat homomorphic encryption on gpus: An implementation using cuda,” *IACR Transactions on Cryptographic Hardware and Embedded Systems*, pp. 70–95, 2018.
- [3] M. R. Albrecht, R. Player, and S. Scott, “On the concrete hardness of learning with errors,” *Cryptography ePrint Archive*, Report 2015/046, 2015, <https://ia.cr/2015/046>.
- [4] P. Barrett, “Implementing the Rivest-Shamir-Adleman public key encryption algorithm on a standard digital signal processor,” in *Advances in Cryptology — CRYPTO’ 86*, A. M. Odlyzko, Ed. Berlin, Heidelberg: Springer Berlin Heidelberg, 1987, pp. 311–323.
- [5] J.-P. Bossuat, C. Mouchet, J. Troncoso-Pastoriza, and J.-P. Hubaux, “Efficient bootstrapping for approximate homomorphic encryption with non-sparse keys,” in *Advances in Cryptology – EUROCRYPT 2021*, A. Canteaut and F.-X. Standaert, Eds. Cham: Springer International Publishing, 2021, pp. 587–617.
- [6] Z. Brakerski, “Fully homomorphic encryption without modulus switching from classical gapsvp,” in *Advances in Cryptology – CRYPTO 2012*, R. Safavi-Naini and R. Canetti, Eds. Berlin, Heidelberg: Springer Berlin Heidelberg, 2012, pp. 868–886.
- [7] Z. Brakerski, C. Gentry, and V. Vaikuntanathan, “(Leveled) fully homomorphic encryption without bootstrapping,” in *ITCS ’12*, 2012.
- [8] Z. Brakerski and V. Vaikuntanathan, “Efficient fully homomorphic encryption from (standard) LWE,” in *IEEE 52nd Annual Symposium on Foundations of Computer Science, FOCS 2011, Palm Springs, CA, USA, October 22–25, 2011*, R. Ostrovsky, Ed. IEEE Computer Society, 2011, pp. 97–106. [Online]. Available: <https://doi.org/10.1109/FOCS.2011.12>
- [9] H. Chen, I. Chillotti, and Y. Song, “Improved bootstrapping for approximate homomorphic encryption,” in *Advances in Cryptology – EUROCRYPT 2019*, Y. Ishai and V. Rijmen, Eds. Cham: Springer International Publishing, 2019, pp. 34–54.
- [10] J. H. Cheon, K. Han, A. Kim, M. Kim, and Y. Song, “Bootstrapping for approximate homomorphic encryption,” in *Annual International Conference on the Theory and Applications of Cryptographic Techniques*. Springer, 2018, pp. 360–384.
- [11] J. H. Cheon, K. Han, A. Kim, M. Kim, and Y. Song, “A full RNS variant of approximate homomorphic encryption,” in *Selected Areas in Cryptography – SAC 2018*, C. Cid and M. J. Jacobson Jr., Eds. Cham: Springer International Publishing, 2019, pp. 347–368.
- [12] J. H. Cheon, A. Kim, M. Kim, and Y. Song, “Homomorphic encryption for arithmetic of approximate numbers,” in *Advances in Cryptology – ASIACRYPT 2017*, T. Takagi and T. Peyrin, Eds. Cham: Springer International Publishing, 2017, pp. 409–437.
- [13] I. Chillotti, N. Gama, M. Georgieva, and M. Izabachène, “Tfhe: fast fully homomorphic encryption over the torus,” *Journal of Cryptology*, vol. 33, no. 1, pp. 34–91, 2020.
- [14] W. Dai and B. Sunar, “cuhe: A homomorphic encryption accelerator library,” in *International Conference on Cryptography and Information Security in the Balkans*. Springer, 2015, pp. 169–186.
- [15] L. de Castro, R. Agrawal, R. T. Yazicigil, A. P. Chandrakasan, V. Vaikuntanathan, C. Juvekar, and A. Joshi, “Does fully homomorphic encryption need compute acceleration?” *CoRR*, vol. abs/2112.06396, 2021. [Online]. Available: <https://arxiv.org/abs/2112.06396>
- [16] L. Deng, “The mnist database of handwritten digit images for machine learning research [best of the web],” *IEEE signal processing magazine*, vol. 29, no. 6, pp. 141–142, 2012.
- [17] L. Ducas and D. Micciancio, “Fhew: bootstrapping homomorphic encryption in less than a second,” in *Annual International Conference on the Theory and Applications of Cryptographic*

- Techniques*. Springer, 2015, pp. 617–640.
- [18] J. Fan and F. Vercauteren, “Somewhat practical fully homomorphic encryption,” *Cryptology ePrint Archive*, Report 2012/144, 2012, <https://ia.cr/2012/144>.
- [19] C. Gentry, *A fully homomorphic encryption scheme*. Stanford university, 2009.
- [20] C. Gentry, S. Halevi, C. Peikert, and N. P. Smart, “Ring switching in bgv-style homomorphic encryption,” in *International Conference on Security and Cryptography for Networks*. Springer, 2012, pp. 19–37.
- [21] J.-Z. Goey, W. K. Lee, B.-M. Goi, and W.-S. Yap, “Accelerating number theoretic transform in gpu platform for fully homomorphic encryption,” *The Journal of Supercomputing*, vol. 77, 02 2021.
- [22] S. Gupta, R. Cammarota, and T. Rosing, “Memfhe: End-to-end computing with fully homomorphic encryption in memory,” *arXiv preprint arXiv:2204.12557*, 2022.
- [23] S. Halevi *et al.*, “Algorithms in helib,” in *Advances in Cryptology – CRYPTO 2014*. Springer, 2014, pp. 554–571.
- [24] S. Halevi, Y. Polyakov, and V. Shoup, “An improved rms variant of the bfv homomorphic encryption scheme,” in *Topics in Cryptology – CT-RSA 2019 - The Cryptographers’ Track at the RSA Conference 2019, Proceedings*, M. Matsui, Ed. Germany: Springer Verlag, 2019, pp. 83–105.
- [25] K. Han, M. Hhan, and J. H. Cheon, “Improved homomorphic discrete fourier transforms and fhe bootstrapping,” *IEEE Access*, vol. 7, pp. 57 361–57 370, 2019.
- [26] K. Han, S. Hong, J. H. Cheon, and D. Park, “Efficient logistic regression on large encrypted data,” *Cryptology ePrint Archive*, 2018.
- [27] K. Han and D. Ki, “Better bootstrapping for approximate homomorphic encryption,” in *Topics in Cryptology – CT-RSA 2020*, S. Jarecki, Ed. Cham: Springer International Publishing, 2020, pp. 364–390.
- [28] D. Hankerson, A. J. Menezes, and S. Vanstone, *Guide to elliptic curve cryptography*. Springer Science & Business Media, 2006.
- [29] “Open source (release 2.2.1),” <https://github.com/homenc/HElib>, Oct. 2021.
- [30] R. Hiromasa, M. Abe, and T. Okamoto, “Packing messages and optimizing bootstrapping in gsw-fhe,” *IEICE TRANSACTIONS on Fundamentals of Electronics, Communications and Computer Sciences*, vol. 99, no. 1, pp. 73–82, 2016.
- [31] W. Jung, S. Kim, J. H. Ahn, J. H. Cheon, and Y. Lee, “Over 100x faster bootstrapping in fully homomorphic encryption through memory-centric optimization with gpus,” *IACR Transactions on Cryptographic Hardware and Embedded Systems*, pp. 114–148, 2021.
- [32] C. Kachris and D. Soudris, “A survey on reconfigurable accelerators for cloud computing,” in *2016 26th International conference on field programmable logic and applications (FPL)*. IEEE, 2016, pp. 1–10.
- [33] A. Kim, “HEAAN,” Online: <https://github.com/snucrypto/HEAAN>, 2018.
- [34] S. Kim, W. Jung, J. Park, and J. H. Ahn, “Accelerating number theoretic transformations for bootstrappable homomorphic encryption on GPUs,” in *2020 IEEE International Symposium on Workload Characterization (IISWC)*. IEEE, 2020, pp. 264–275.
- [35] S. Kim, J. Kim, M. J. Kim, W. Jung, M. Rhu, J. Kim, and J. H. Ahn, “Bts: An accelerator for bootstrappable fully homomorphic encryption,” *arXiv preprint arXiv:2112.15479*, 2021.
- [36] “Lattigo 1.3.0,” Online: <http://github.com/ldsec/lattigo>, Dec. 2019, ePFL-LDS.
- [37] A. Munshi, “The opencl specification,” in *2009 IEEE Hot Chips 21 Symposium (HCS)*. IEEE, 2009, pp. 1–314.
- [38] A. Norton and A. J. Silberger, “Parallelization and performance analysis of the cooley? tukey fft algorithm for shared-memory architectures,” *IEEE Transactions on Computers*, vol. 36, no. 05, pp. 581–591, 1987.
- [39] M. S. Riazi, K. Laine, B. Pelton, and W. Dai, “Heax: An architecture for computing on encrypted data,” in *Proceedings of the Twenty-Fifth International Conference on Architectural Support for Programming Languages and Operating Systems*, 2020, pp. 1295–1309.
- [40] R. L. Rivest, L. Adleman, and M. L. Dertouzos, “On data banks and privacy homomorphisms,” *Foundations of Secure Computation*, Academia Press, pp. 169–179, 1978.
- [41] N. Samardzic, A. Feldmann, A. Krastev, S. Devadas, R. Dreslinski, C. Peikert, and D. Sanchez, “F1: A fast and programmable accelerator for fully homomorphic encryption,” in *MICRO-54: 54th Annual IEEE/ACM International Symposium on Microarchitecture*, 2021, pp. 238–252.
- [42] “Microsoft SEAL (release 3.7),” <https://github.com/Microsoft/SEAL>, Sep. 2021, microsoft Research, Redmond, WA.
- [43] D. Technologies, “PALISADE library,” Online: <https://gitlab.com/palisade/palisade-release>, 2019.
- [44] M. A. Will and R. K. Ko, “Computing mod without mod,” *Cryptology ePrint Archive*, 2014.
- [45] Y. Zhai, M. Ibrahim, Y. Qiu, F. Boemer, Z. Chen, A. Titov, and A. Lyashevsky, “Accelerating Encrypted Computing on Intel GPUs,” *ArXiv*, 2021.
- [46] C. Zhang, M. Yu, W. Wang, and F. Yan, “[Mark]: Exploiting cloud services for {Cost-Effective}, {SLO-Aware} machine learning inference serving,” in *2019 USENIX Annual Technical Conference (USENIX ATC 19)*, 2019, pp. 1049–1062.